

Article

# Formation Mechanism of Porous Cu<sub>3</sub>Sn Intermetallic Compounds by High Current Stressing at High Temperatures in Low-Bump-Height Solder Joints

Jie-An Lin <sup>1</sup>, Chung-Kuang Lin <sup>1</sup>, Chen-Min Liu <sup>1</sup>, Yi-Sa Huang <sup>1</sup>, Chih Chen <sup>1,\*</sup>, David T. Chu <sup>2</sup> and King-Ning Tu <sup>2</sup>

Received: 22 November 2015; Accepted: 11 January 2016; Published: 16 January 2016

Academic Editor: Duc Nguyen-Manh

<sup>1</sup> Department of Materials Science and Engineering, National Chiao Tung University, Hsinchu 30010, Taiwan; james77633@yahoo.com.tw (J.-A.L.); inferng@yahoo.com.tw (C.-K.L.); amin6397@yahoo.com.tw (C.-M.L.); isaacbear1225@gmail.com (Y.-S.H.)

<sup>2</sup> Department of Materials Science and Engineering, University of California at Los Angeles, Los Angeles, CA 90095-1595, USA; davidtaweichu@gmail.com (D.T.C.); kntu@ucla.edu (K.-N.T.)

\* Correspondence: chih@mail.nctu.edu.tw; Tel.: +886-3-5731814; Fax: +886-3-5724727

**Abstract:** Electromigration tests of SnAg solder bump samples with 15 μm bump height and Cu under-bump-metallization (UBM) were performed. The test conditions were  $1.45 \times 10^4$  A/cm<sup>2</sup> at 185 °C and  $1.20 \times 10^4$  A/cm<sup>2</sup> at 0 °C. A porous Cu<sub>3</sub>Sn intermetallic compound (IMC) structure was observed to form within the bumps after several hundred hours of current stressing. In direct comparison, annealing alone at 185 °C will take more than 1000 h for porous Cu<sub>3</sub>Sn to form, and it will not form at 170 °C even after 2000 h. Here we propose a mechanism to explain the formation of this porous structure assisted by electromigration. The results show that the SnAg bump with low bump height will become porous-type Cu<sub>3</sub>Sn when stressing with high current density and high temperature. Polarity effects on porous Cu<sub>3</sub>Sn formation is discussed.

**Keywords:** intermetallic compounds; porous Cu<sub>3</sub>Sn; electromigration; side wall reaction

## 1. Introduction

In the pursuit of higher operation speed and improved performance of microelectronic devices [1], the application of flip chip solder joints has become a key technology for high-density packaging. The solder joints have been used in high power devices, such as central processing unit (CPU) and application processors (AP). The specification of operation temperatures for these devices range from 100 to 110 °C and the required lifetime is usually 10 years. To meet the demand for portable devices, the input/output pin numbers continue to increase while the size of the solder joints continues to shrink. This inevitably leads to higher current densities and operating temperatures in the joints. Therefore, it raises serious reliability issues such as electromigration and thermomigration [2].

Over the past decades, electromigration behavior and metallurgical reactions of flip chip solder joints have been widely studied [3–9]. The intermetallic compounds (IMC) of Cu<sub>3</sub>Sn and Cu<sub>6</sub>Sn<sub>5</sub> are commonly formed in solder reactions on Cu under-bump-metallization (UBM). The Cu column-type UBM (a structure with a thicker Cu) was developed to alleviate both the Joule heating and current crowding effects in flip-chip solder joints under normal device operating conditions, having a longer lifetime [10].

Dimensional shrinkage of the solder joints in portable devices may cause new reliability issues. The smaller solder joints tend to transform completely into IMC joints during electromigration tests [11]. Additionally, in low-bump-height solder joints, when they are combined with a thick column-type Cu

UBM, the solder reaction on the side wall of the Cu-column becomes one of the new reliability issues of concern. Liang *et al.* found that in reflow tests, the effect of side wall reaction would lead to the formation of large voids in the solder joints [12].

Panchenko *et al.* reported a porous  $\text{Cu}_3\text{Sn}$  structure in 50  $\mu\text{m}$  pitch Cu/Sn microbump interconnects during reflow due to the degradation of the  $\text{Cu}_6\text{Sn}_5$  IMCs layer [13]. The proposed explanation of the porous  $\text{Cu}_3\text{Sn}$  formation is the dissolution of Sn atoms from the  $\text{Cu}_6\text{Sn}_5$  matrix owing to the reaction between  $\text{Cu}_6\text{Sn}_5$  and flux residues. However, the formation mechanism of the porous  $\text{Cu}_3\text{Sn}$  structure has not yet been confirmed.

In this study, we investigated the microstructure evolution of solder joints with Cu column UBM, especially the porous  $\text{Cu}_3\text{Sn}$  formation, under current stressing at  $1.45 \times 10^4 \text{ A/cm}^2$  at 185 °C and  $1.20 \times 10^4 \text{ A/cm}^2$  at 170 °C. We observed the porous  $\text{Cu}_3\text{Sn}$  formation enhanced by current stressing.

## 2. Experimental Methods

Typical flip-chip solder joints were used in our electromigration tests. Figure 1a shows the schematic diagram of a bump with Cu column UBM. On the chip side, 100 nm Ti was sputtered as the adhesion layer. Then a 2  $\mu\text{m}$  Cu layer was sputtered as the seed layer for the subsequent electroplating of a 50  $\mu\text{m}$  Cu UBM column and SnAg solder. The composition of the solder was Sn-2.3Ag. The diameter of UBM and passivation opening is 145 and 85  $\mu\text{m}$ , respectively. The Cu trace on the flame retardant 5 (FR5) substrate is 100  $\mu\text{m}$  wide and 27  $\mu\text{m}$  thick. Pre-solder of Sn-2.3Ag was used on the substrate side. The chips were flipped over to align with the substrates, and they were reflowed at 260 °C for 1 min to form flip-chip solder joints. Figure 1b illustrates the cross-sectional SEM images of a flip-chip bump before the Electromigration EM tests. A scallop-type  $\text{Cu}_6\text{Sn}_5$  layer was found at the interface between the Cu metallization and the solder on the chip side, as well as on the substrate side [14].

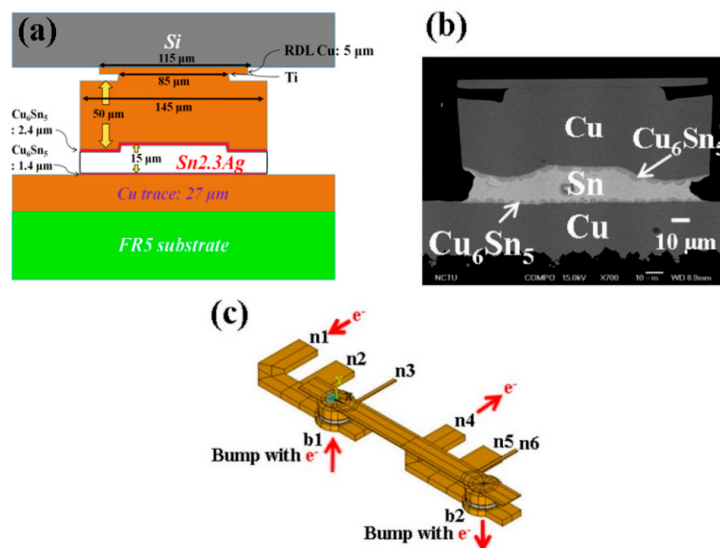


**Figure 1.** (a) Schematic of the flip-chip solder joints with Cu column UBM. The redistribution layer (RDL) on the Si chip is 5- $\mu\text{m}$  thick Cu; (b) Cross-sectional SEM images; (c) Layout for electromigration tests and four-point structure for measuring bump resistance.

Four-point probes were employed to monitor the resistance change during the EM tests of the bump. Figure 1c presents the schematic of the test layout. There are 6 nodes (n1 to n6) in the test layout, and the direction of the electron flow is pointed by the red arrows which shows the two bumps (b1 and b2) were stressed with opposite direction of electron flow. The electrons enter from n1, go upward through b1, then downward through b2, and finally flow out from n6. The resistance change in b1 (b2) can be measured by the voltage drop between n2 and n3 (n5 and n6). In the microelectronic industry, a

failure is typically defined when the resistance change increases to 20% of its initial value [15]. In our study, the early stage of the tests was defined when the bump resistance increment is smaller than 20% during the EM tests, while the later stage of test was defined when the increment was larger than 20%.

The solder joints were stressed with 2.4 A and 2 A at 150 °C. The calculated current densities were  $1.45 \times 10^4$  A/cm<sup>2</sup> and  $1.20 \times 10^4$  A/cm<sup>2</sup>, respectively, based on the UBM opening size. The real temperature in solder joints may be higher than the ambient temperature during current stressing due to Joule heating effect in the stressing condition [6]. Therefore, in our study the temperature coefficient of resistivity (TCR) were employed to measure the real temperature in the joints. The calibrated temperatures were about 185 °C and 170 °C when the test sample was stressed with 2.4 and 2 A, respectively.

Solder joints were cross-sectioned by grinding using abrasive papers #400, #1000, #2000, #2500, and #4000, and then polished by Al<sub>2</sub>O<sub>3</sub> of 1 and 0.3 μm. The microstructure and composition were examined with a JEOL 6500 field-emission scanning electron microscope (SEM) (JEOL Ltd., Tokyo, Japan) and energy dispersive spectroscopy (EDS) (Oxford Instruments, Oxfordshire, UK). The SEM EDS was operated at 15 KeV with a current of  $1.0 \times 10^{-5}$  A and a beam size of 1000 nm. Focused ion beam (FIB, FEI Nova 200, FEI Company, Hillsboro, OR, USA) technique was adopted for cross-sectional observation, and transmission electron microscopy (TEM, JEOL-2100F, JEOL Ltd., Tokyo, Japan) and electron probe micro-analyzer (EPMA, JXA-8800M, JEOL Ltd., Tokyo, Japan) were utilized to verify the microstructure results. The operation conditions for the EPMA were at 12 KeV with a current of  $1.0 \times 10^{-8}$  A and a beam size of 500 nm.

### 3. Results and Discussion

#### 3.1. Current-Enhanced IMC Formation

The formation of Cu-Sn IMCs can be significantly enhanced by current stressing. Figure 2 shows cross-sectional SEM images of a pair of solder joints stressed with  $1.45 \times 10^4$  A/cm<sup>2</sup> at 185 °C. At the early stage, the bump resistance increased by 5% (after 283 h in the upward electron flow) and 10% (after 283 h in the downward electron flow) of its initial value, are shown in Figure 2a,b, respectively. The current enhanced the dissolution of Cu UBM to react with the solder joint and form a large volume of IMCs. The layer-type Cu<sub>6</sub>Sn<sub>5</sub> formed in the middle of the bump and the layer-type Cu<sub>3</sub>Sn formed at the interfaces between the Cu and Cu<sub>6</sub>Sn<sub>5</sub>. The entire joint almost completely transformed into IMC joints at the early stage in the EM tests, although there was still some Sn remaining in the bump, as indicated in Figure 2b. The results showed that a large volume of IMCs formed at the early stage regardless of the direction of the electron flow.

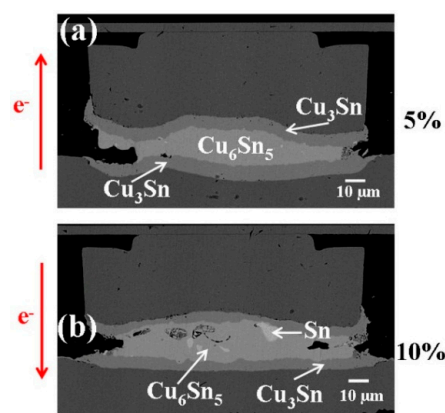


**Figure 2.** Cross-sectional SEM images of solder bumps with Cu column UBM stressed at  $1.45 \times 10^4$  A/cm<sup>2</sup> at 185 °C with bump resistance increases (a) 5% with upward electron flow and (b) 10% with downward electron flow.

### 3.2. Formation of Porous $\text{Cu}_3\text{Sn}$

It is interesting that porous  $\text{Cu}_3\text{Sn}$  IMCs may form at later stages of electromigration tests. Figures 3 and 4 illustrate the cross-sectional SEM images at different stages in the EM tests with opposite direction of electron flow. Figure 3 shows the EM test results with upward electron flow. Figure 3a–c are the cross-sectional SEM images with bump resistance increase, 8% (after 517 h), 32% (after 217 h), and 85% (after 429 h) of its initial value, respectively. When the bump resistance increased to 8% of its initial value, the layer-type  $\text{Cu}_6\text{Sn}_5$  in the middle started to transform into porous-type  $\text{Cu}_3\text{Sn}$ , as shown in Figure 3a. We note that the porous-type  $\text{Cu}_3\text{Sn}$  first formed on the periphery of the bump. As the change in bump resistance increased to 32%, shown in Figure 3b, the layer-type  $\text{Cu}_6\text{Sn}_5$  IMC had fully transformed into porous-type  $\text{Cu}_3\text{Sn}$  IMC. Figure 3c shows similar results, from a different bump, as Figure 3b which means the  $\text{Cu}_6\text{Sn}_5$  IMC had also totally transformed into porous-type  $\text{Cu}_3\text{Sn}$  IMCs in the later stage of the EM tests.

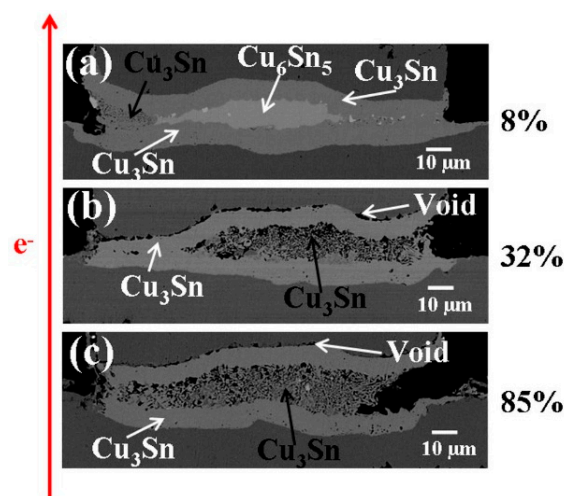


**Figure 3.** Cross-sectional SEM images of solder bumps with Cu column UBM stressed at  $1.45 \times 10^4 \text{ A/cm}^2$  with upward electron flow at  $185 \text{ }^\circ\text{C}$  with bump resistance increases (a) 8%, (b) 32%, and (c) 85% of its initial value.

Similarly, Figure 4 shows the EM tests results with downward electron flow, where Figure 4a–c illustrate the cross-sectional SEM images with the bump resistance increase 15% (after 517 h), 20% (after 217 h), and 100% (after 429 h) of its initial value, respectively. The results are similar to those in Figure 3. As the bump resistance increased, the layer-type  $\text{Cu}_6\text{Sn}_5$  in the middle started to transform into porous-type  $\text{Cu}_3\text{Sn}$ .

In order to rule out the possibility that the porous structure was generated in the polishing process or by other external forces, FIB were utilized to provide a deeper cross-section in a selected solder joint, stressed at  $1.45 \times 10^4 \text{ A/cm}^2$  for 429 h as illustrated in Figure 5. The downward direction of the electron flow was labeled in the figure. This second cross-section view indicated that the porous structure not only formed on the polished surface but in the entire bump.

In the bumps with porous  $\text{Cu}_3\text{Sn}$ , we observed that the effect of side wall reaction is very serious. Park *et al.* reported that a high stressing current may lead to a serious side wall reaction effect [16]. Figure 6a shows the side wall of a bump. The bump has had porous-type  $\text{Cu}_3\text{Sn}$  IMCs formation. We can clearly observe that there are IMCs formation on the side wall, indicated by the ellipses. Since the thickness of the IMCs formed on the side wall is only about  $3 \text{ }\mu\text{m}$ , it is hard to verify the composition with EDS. Hence, EPMA was used instead. Figure 6b illustrates the results that all the IMCs formed on the side wall are  $\text{Cu}_3\text{Sn}$ . The compositions of the layer-type and porous-type structures were also confirmed with EPMA to be  $\text{Cu}_3\text{Sn}$ , identical with the results measured with EDS. Therefore, the whole joint has transformed completely into  $\text{Cu}_3\text{Sn}$  with two different morphologies.

Figure 7 shows the cross-sectional TEM image and the electron diffraction patterns of point “a” in a porous  $\text{Cu}_3\text{Sn}$ . In the diffraction pattern, the spots correspond to the principle reflections of a basic hexagonal lattice. The zone axes are indexed with  $[01\bar{1}2]$ . The results show that the porous-type structure is hexagonal  $\text{Cu}_3\text{Sn}$ .

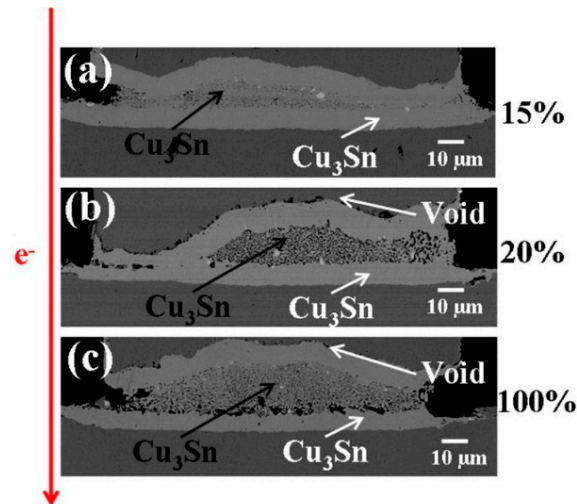


**Figure 4.** Cross-sectional SEM images of solder bumps with Cu column UBM stressed at  $1.45 \times 10^4 \text{ A/cm}^2$  with downward electron flow at  $185 \text{ }^\circ\text{C}$  with bump resistance increases (a) 15%, (b) 20%, and (c) 100% of its initial value. Cross-sectional SEM images of solder bumps with Cu column UBM stressed at  $1.45 \times 10^4 \text{ A/cm}^2$  with downward electron flow at  $185 \text{ }^\circ\text{C}$  with bump resistance increases (a) 15%, (b) 20%, and (c) 100% of its initial value.

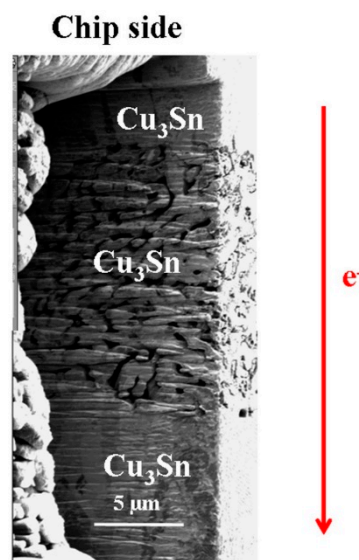


**Figure 5.** Cross-sectional FIB image of  $\text{Cu}_3\text{Sn}$  IMC structures.

To determine the conditions under which porous  $\text{Cu}_3\text{Sn}$  could form, we stressed the sample at a lower current density and, hence, a lower temperature. Figure 8 shows cross-sectional SEM images of a pair of solder joints stressed with  $1.2 \times 10^4 \text{ A/cm}^2$  at  $170 \text{ }^\circ\text{C}$ . The bump resistance increases 140% (after 5094 h) and 530% (after 5094 h) of its initial value as indicated in Figure 8a,b, respectively. It can be seen that only layer-type  $\text{Cu}_3\text{Sn}$  and layer-type  $\text{Cu}_6\text{Sn}_5$  have formed, with no evidence of porous  $\text{Cu}_3\text{Sn}$  even in the case of Figure 8b. The results demonstrate that the solder joints do not transform into porous structures at an insufficient current density and temperature.

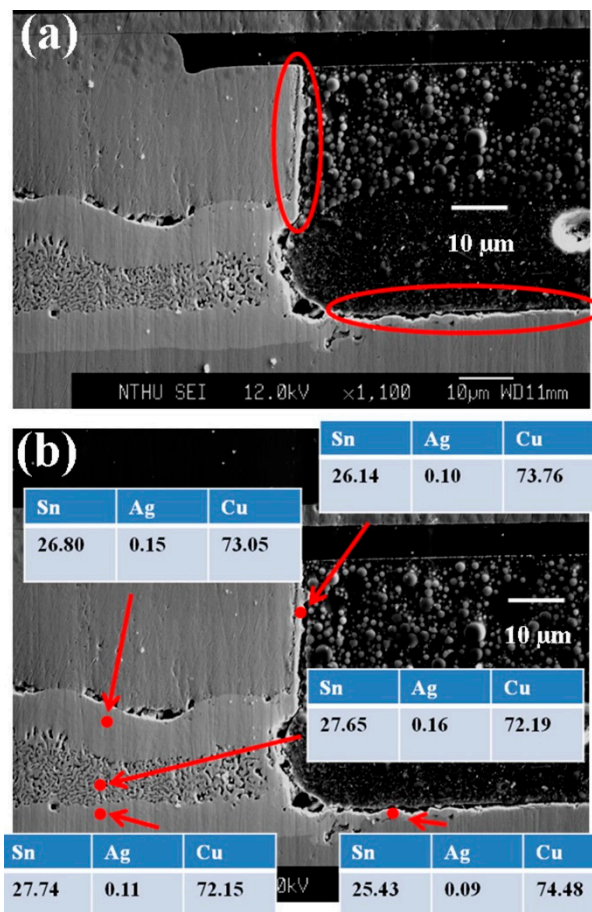


**Figure 6.** Cross-sectional SEM images of (a) IMCs formed on the side wall and (b) EPMA analysis. The composition data were shown in atomic percent.

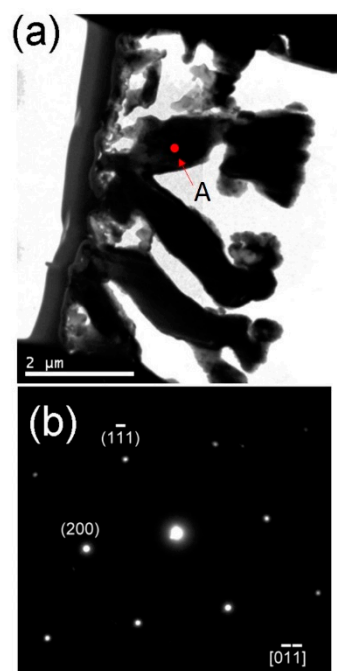


**Figure 7.** (a) Cross-sectional TEM image of porous-type structure and (b) diffraction patterns of point A in (a).

To further examine the temperature effect on the of porous  $\text{Cu}_3\text{Sn}$  formation, another set of bumps were aged at  $185^\circ\text{C}$  in the oven without current stressing. In the case of 1000-h aging (Figure 9a), the joints have fully transformed into IMC joints. Layer-type  $\text{Cu}_6\text{Sn}_5$  has formed in the middle of the bump and layer-type  $\text{Cu}_3\text{Sn}$  has formed between Cu and  $\text{Cu}_6\text{Sn}_5$ . In the case of 2000 h aging (Figure 9b), the layer-type  $\text{Cu}_6\text{Sn}_5$  in the middle has completely transformed into porous  $\text{Cu}_3\text{Sn}$ . The results show that porous  $\text{Cu}_3\text{Sn}$  could form without current stressing at a sufficiently high temperature, which gives an independent confirmation of temperature's critical role in the formation of porous  $\text{Cu}_3\text{Sn}$ .

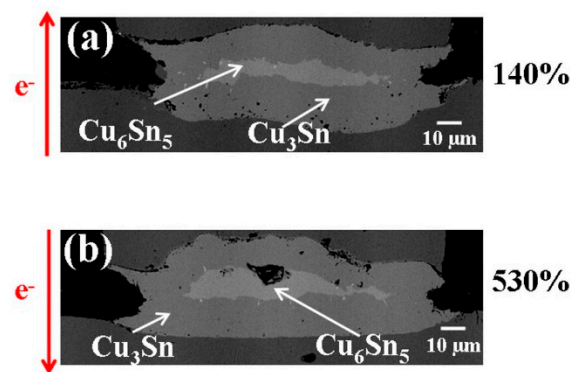


**Figure 8.** Cross-sectional SEM images of solder bumps with Cu column UBM stressed at  $1.20 \times 10^4 \text{ A/cm}^2$  at  $170^\circ\text{C}$  with bump resistance increases (a) 140% with upward electron flow and (b) 530% with downward electron flow.

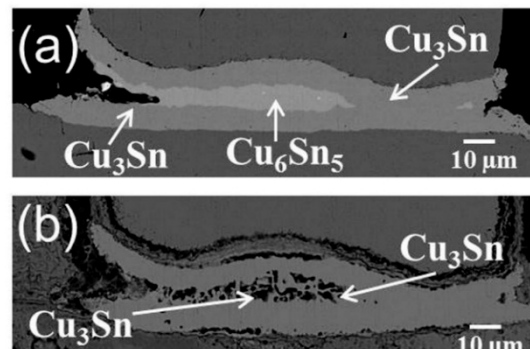


**Figure 9.** Cross-sectional SEM images of solder bumps with Cu column UBM aging at  $185^\circ\text{C}$  for (a) 1000 h and (b) 2000 h.

So far, we have observed that the porous-type  $\text{Cu}_3\text{Sn}$  IMCs can form during high current stressing at high temperatures and the effect of side wall wetting is obvious. To explain its formation mechanism, a further discussion is presented in the next section.

### 3.3. Formation Mechanism of Porous $\text{Cu}_3\text{Sn}$ IMCs

On the formation mechanism of porous  $\text{Cu}_3\text{Sn}$ , first, the temperature must be high enough. Second, the solder height must be low enough so that the Cu supply is enough for the whole joint to transform into IMC. This is because when there are unreacted solders in the joints, the major IMC is  $\text{Cu}_6\text{Sn}_5$  after the metallurgical reactions, as illustrated in Figure 1b. Only a thin layer of  $\text{Cu}_3\text{Sn}$  presented between the Cu metallization layer and the  $\text{Cu}_6\text{Sn}_5$  IMCs. The transformation process is schematically illustrated in Figure 10. In the early stage of the EM tests, layer-type  $\text{Cu}_6\text{Sn}_5$  and  $\text{Cu}_3\text{Sn}$  formed first, as shown in Figure 10a. As the bump resistance increased, the layer-type  $\text{Cu}_6\text{Sn}_5$  started to transform into porous-type  $\text{Cu}_3\text{Sn}$ , as illustrated in Figure 10b. The IMCs formed on the side walls due to the effect of side wall reaction are also shown in Figure 10b, labeled by the ellipses.

According to the experimental results, we have developed the following mechanism to explain the formation of the porous-type  $\text{Cu}_3\text{Sn}$ . Previously, the Kirkendall void formation mechanism in  $\text{Cu}_3\text{Sn}$  was proposed [17]. When the layer-type  $\text{Cu}_6\text{Sn}_5$  decomposes into  $\text{Cu}_3\text{Sn}$ , it will release 3 Sn atoms:



The Sn atoms will then attract nine Cu atoms to form three more  $\text{Cu}_3\text{Sn}$ .

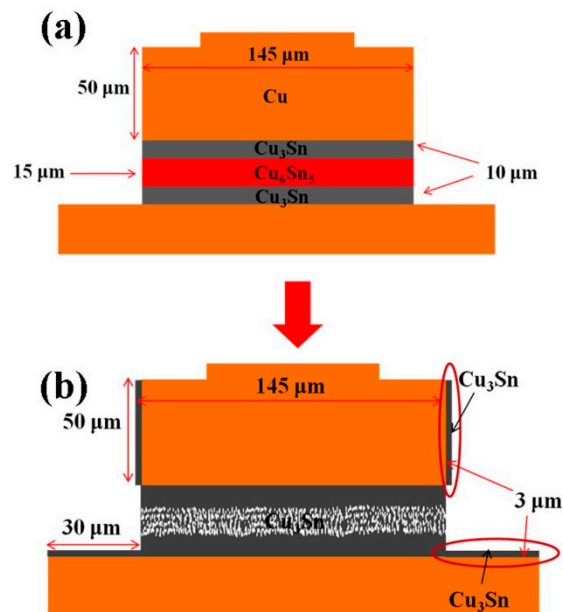
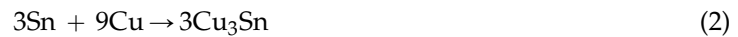


**Figure 10.** Schematic diagrams of transformation process at (a) early stage and (b) final stage in the electromigration tests.

The vacancies which enable the diffusion of the Cu atoms tend to form Kirkendall voids in  $\text{Cu}_3\text{Sn}$ . It implies that the growth of layer-type  $\text{Cu}_3\text{Sn}$  IMCs is at the expense of layer-type  $\text{Cu}_6\text{Sn}_5$  IMCs. However, in our experimental results, it can be observed that as the layer-type  $\text{Cu}_3\text{Sn}$  IMCs grew to certain thickness, the layer-type  $\text{Cu}_6\text{Sn}_5$  would not transform into the layer-type but porous-type  $\text{Cu}_3\text{Sn}$ . Hsiao *et al.* found that Cu-Sn IMCs can become a diffusion barrier for the Cu/solder reaction [18]. We assume that the layer-type  $\text{Cu}_3\text{Sn}$  served as a diffusion barrier and inhibited the Sn atoms released from the decomposition of  $\text{Cu}_6\text{Sn}_5$  to react with Cu. Since the bumps were stressed with high current density at high temperature, the released Sn diffused to the side wall to form  $\text{Cu}_3\text{Sn}$  due to the effect of the side wall reaction. The place originally occupied by Sn became empty and led to the porous-type structure.

#### 3.4. Polarity Effect

We have observed the polarity effect in the final stage of the EM tests; namely, more porous structures formed on the anode side than on the cathode side. By the mechanism theorized above, the phenomenon was caused by an abundant Cu supply on the cathode side than on the anode side. Hence, there was more  $\text{Cu}_3\text{Sn}$  formation on the cathode side. However, Cu atoms were less likely to diffuse to the anode side to react with the released Sn. As a result, the porous structure was more obvious on the anode side. The polarity effect is, thus, a consequence of the proposed mechanism.

### 3.5. Theoretical Calculation of Pore Volume

This mechanism can be further verified by volume calculations. One mole of  $\text{Cu}_6\text{Sn}_5$  decomposes into two moles of  $\text{Cu}_3\text{Sn}$  plus three moles of Sn. Approximately, one mole of  $\text{Cu}_6\text{Sn}_5$  has a volume of  $117.7 \text{ cm}^3$ , two moles of  $\text{Cu}_3\text{Sn}$  has a volume of  $69.5 \text{ cm}^3$ , and three moles of Sn has a volume of  $48.4 \text{ cm}^3$ . In our observation, the volume before and after the  $\text{Cu}_6\text{Sn}_5$  to  $\text{Cu}_3\text{Sn}$  conversion was nearly unchanged ( $117.7$  to  $117.9 \text{ cm}^3$ ). Calculations also indicate that the volume change in phase transformation is negligible. On the other hand, the diffusion of Sn to the side walls would leave the pores behind. Assuming that the pore volume equals that of the released Sn, we have calculated the volume occupied by pores to be 41.2% ( $48.4/117.9$ ) of the porous  $\text{Cu}_3\text{Sn}$  volume, when all the released Sn atoms diffuse to the side walls of the UBMs. As a verification, we have used software to calculate the volume percentage of the pores in the actual bumps. Six bumps were input into the software to ensure accuracy. The average volume percentage of the pores was found to be 38.2%, a number close to the theoretical 41.2%. The volume of pores (or the volume of the released Sn) in the bumps is approximately  $63,879 \mu\text{m}^3$ . We assume that all of released Sn atoms have diffused to the side walls to form  $\text{Cu}_3\text{Sn}$ . This implies that  $63,879 \mu\text{m}^3$  of Sn would form  $137,978 \mu\text{m}^3$  of  $\text{Cu}_3\text{Sn}$  on the side walls. This is again close to the calculated value of  $157,932 \mu\text{m}^3$  for the volume of  $\text{Cu}_3\text{Sn}$  formed on the side walls in the actual bumps.

The above experimental results and calculation both indicate Sn diffusion to side walls of Cu UBM may be a possible mechanism for the formation of the porous  $\text{Cu}_3\text{Sn}$ . The porous  $\text{Cu}_3\text{Sn}$  will be a reliability issue for solder joints with Cu UBM. Yet, no solutions have been proposed so far to prevent it from happening. More studies need to be performed to solve this problem.

## 4. Conclusions

We have carried out a systematic study on an important reliability issue related to high-density packaging of microelectronic devices. In this study, SnAg solder bump samples with Cu UBM were stressed at current densities of  $1.45 \times 10^4 \text{ A/cm}^2$  and  $1.20 \times 10^4 \text{ A/cm}^2$  and operating temperatures of approximately  $185 \text{ }^\circ\text{C}$  and  $170 \text{ }^\circ\text{C}$ , respectively. A porous  $\text{Cu}_3\text{Sn}$  structure, unseen in traditional flip-chip solder joints, was observed in the process.  $\text{Cu}_3\text{Sn}$  IMCs were also observed on the side walls of Cu column UBM due to side wall reactions. We have proposed a theory to explain the formation mechanism of the observed porous  $\text{Cu}_3\text{Sn}$  and side-wall  $\text{Cu}_3\text{Sn}$ . In the reaction:  $\text{Cu}_6\text{Sn}_5 \rightarrow 2\text{Cu}_3\text{Sn} + 3\text{Sn}$ , one  $\text{Cu}_6\text{Sn}_5$  molecule converted into three  $\text{Cu}_3\text{Sn}$  molecules and three Sn atoms were released. The released Sn left pores behind to form the porous  $\text{Cu}_3\text{Sn}$ . This is because when the early formed layer-type  $\text{Cu}_3\text{Sn}$  becomes a barrier to Cu diffusion, the released Sn atoms, taking an alternative path, diffuse to the side walls to form the  $\text{Cu}_3\text{Sn}$  IMCs by side wall reaction. Results of volume calculations were consistent with the proposed processes and consequently provided further evidence of this mechanism. In the past, the layer-type  $\text{Cu}_3\text{Sn}$  is regarded as the terminal phase for the solid-state Cu-Sn reactions; however, our results conclude that the SnAg bump with low bump height would lead to porous-type  $\text{Cu}_3\text{Sn}$  formation when it is stressed with high current densities and high temperatures.

**Acknowledgments:** Financial support from the Ministry of Science and Technology, Taiwan, under the contract of 101-2628-E-009-017-MY3 is acknowledged.

**Author Contributions:** J.-A.L. contributed to electromigration tests and co-wrote the paper. C.-K.L. contributed electromigration tests and SEM analysis. C.-M.L. contributed to TEM analysis. Y.-S.H. contributed to TEM sample preparation. D.T.C. contributes to void analysis and discussion. C.C. and K.-N.T. led the study and co-wrote the paper.

**Conflicts of Interest:** The authors declare no conflict of interest.

## References

1. Tu, K.N. Recent advances on electromigration in very-large-scale-integration of interconnects. *J. Appl. Phys.* **2003**, *94*, 5451–5473. [[CrossRef](#)]

2. Chen, C.; Tong, H.M.; Tu, K.N. Electromigration and Thermomigration in Pb-Free Flip-Chip Solder Joints. *Rev. Mater. Sci.* **2010**, *40*, 531–555. [[CrossRef](#)]
3. Chen, C.; Liang, S.W. Electromigration issues in lead-free solder joints. *J. Mater. Sci. Mater. Electron.* **2007**, *18*, 259–268. [[CrossRef](#)]
4. Chu, M.H.; Liang, S.W.; Chen, C.; Huang, A.T. Electromigration Failure Mechanism in Sn-Cu Solder Alloys with OSP Cu Surface Finish. *J. Electron. Mater.* **2012**, *41*, 2502–2507. [[CrossRef](#)]
5. Zeng, K.; Tu, K.N. Six cases of reliability study of Pb-free solder joints in electronic packaging technology. *Mater. Sci. Eng. R Rep.* **2002**, *38*, 55–105. [[CrossRef](#)]
6. Chiu, S.H.; Chen, C. Investigation of void nucleation and propagation during electromigration of flip-chip solder joints using x-ray microscopy. *Appl. Phys. Lett.* **2006**, *89*. [[CrossRef](#)]
7. Liu, C.Y.; Chen, C.; Liao, C.N.; Tu, K.N. Microstructure-electromigration correlation in a thin stripe of eutectic SnPb solder stressed between Cu electrodes. *Appl. Phys. Lett.* **1999**, *75*, 58–60. [[CrossRef](#)]
8. Liang, S.W.; Chang, Y.W.; Shao, T.L.; Chen, C.; Tu, K.N. Effect of three-dimensional current and temperature distributions on void formation and propagation in flip-chip solder joints during electromigration. *Appl. Phys. Lett.* **2006**, *89*, 022117. [[CrossRef](#)]
9. Liang, S.W.; Chiu, S.H.; Chen, C. Effect of Al-trace degradation on Joule heating during electromigration in flip-chip solder joints. *Appl. Phys. Lett.* **2007**, *90*, 082103. [[CrossRef](#)]
10. Liang, Y.C.; Tsao, W.A.; Chen, C.; Yao, D.; Huang, A.T.; Lai, Y. Influence of Cu column under-bump-metallizations on current crowding and Joule heating effects of electromigration in flip-chip solder joints. *J. Appl. Phys.* **2012**, *111*, 043705. [[CrossRef](#)]
11. Xu, L.; Han, J.; Liang, J.J.; Tu, K.N.; Lai, Y. Electromigration induced high fraction of compound formation in SnAgCu flip chip solder joints with copper column. *Appl. Phys. Lett.* **2008**, *92*, 262104. [[CrossRef](#)]
12. Liang, Y.C.; Chen, C.; Tu, K.N. Side Wall Wetting Induced Void Formation due to Small Solder Volume in Microbumps of Ni/SnAg/Ni upon Reflow. *ECS Solid State Lett.* **2012**, *1*, 60–62. [[CrossRef](#)]
13. Panchenko, I.; Croes, K.; Wolf, I.D.; Messemaeker, J.D.; Beyne, E.; Wolter, K. Degradation of Cu<sub>6</sub>Sn<sub>5</sub> intermetallic compound by pore formation in solid-liquid interdiffusion Cu/Sn microbump interconnects. *Microelectron. Eng.* **2014**, *117*, 26–34. [[CrossRef](#)]
14. Tu, K.N. *Solder Joint Technology*; Springer: New York, NY, USA, 2007.
15. Joint Electron Device Engineering Council (JEDEC). *Guideline for Characterizing Solder Bump Electromigration Under Constant Current and Temperature Stress*; JEDEC Standard JEP154; JEDEC: Arlington, VA, USA, 2008.
16. Park, Y.; Kim, S.; Park, J.; Kim, J.; Son, H.; Han, K.; Oh, J.; Kim, N.; Yoo, S. Current Density Effects on the Electrical Reliability of Ultra Fine-Pitch Micro-Bump for TSV Integration. In Proceedings of the 2013 IEEE 63rd Electronic Components and Technology Conference, Las Vegas, NV, USA, 28–31 May 2013.
17. Zeng, K.; Stierman, R.; Chiu, T.; Edwards, D.; Ano, K.; Tu, K.N. Kirkendall void formation in eutectic SnPb solder joints on bare Cu and its effect on joint reliability. *J. Appl. Phys.* **2005**, *97*, 024508. [[CrossRef](#)]
18. Hsiao, H.Y.; Hu, C.; Guo, M.; Chen, C.; Tu, K.N. Inhibiting the consumption of Cu during multiple reflows of Pb-free solder on Cu. *Scr. Mater.* **2011**, *65*, 907–910. [[CrossRef](#)]

